Contents lists available at ScienceDirect

Atmospheric Research

An environmental synoptic analysis of tropical transitions in the central and Eastern North Atlantic

C. Calvo-Sancho [a,*], J.J. González-Alemán [b], P. Bolgiani [c], D. Santos-Muñoz [d], J.I. Farrán [a], M. L. Martín [a,e]

[a] Department of Applied Mathematics, Faculty of Computer Engineering, University of Valladolid, Segovia, Spain
[b] Agencia Estatal de Meteorología (AEMET), Madrid, Spain
[c] Department of Earth Physics and Astrophysics, Faculty of Physics, Complutense University of Madrid, Madrid, Spain
[d] Danmarks Meteorologiske Institute, Denmark
[e] Institute of Interdisciplinary Mathematics (IMI), Complutense University of Madrid, Madrid, Spain

ARTICLE INFO

ABSTRACT

A tropical transition (TT) is the process whereby a baroclinic, high-to-moderate vertical wind shear, extratropical or subtropical cyclone is transformed into a warm-core, low vertical wind shear, tropical cyclone. Thirty TT events were identified over the central and eastern North Atlantic basin during the period 1979–2019. The TT process is here studied from a synoptic storm-centered composite climatology and an environmental classification perspective. The aim is to study their common features and highlight their differences. The storm-centered composite analysis reveals that a westerlies meridional trough with quasigeostrophic forcig acts as precursor. TT environments are characterized by a trough at 300 hPa geopotential and the increase of the 1000–500 hPa thickness, i.e., the system evolves into a warm-core, and a strong anticyclone is located north of the surface cyclone. The transition is accompanied by a large latent heat release which promotes the vertical redistribution of potential vorticity and a reduction of the 850–300 hPa vertical wind shear. The identified TTs in the central North Atlantic predominantly developed in environments with warm sea surface temperatures (> 25 °C) and low-to-moderate wind shear (10–15 m s^{-1}). In contrast, the eastern North Atlantic TTs transitioned in low sea surface temperature values (< 25 °C) and high wind shear (> 15 m s^{-1}). Finally, the statistically significant differences in the environmental classification encouraged further analysis of their environments via storm-centered composites, revealing that eastern North Atlantic cyclones have a more defined extratropical structure, while central North Atlantic cyclones show more tropical characteristics.

1. Introduction

Tropical cyclones (TCs) are associated with high impact to the general population and ecological systems. These impacts cover a wide range of damage, from agriculture and human losses to tourism and infrastructures, including security issues and environmental hazards (Peduzzi et al., 2012; Lenzen et al., 2019). Tropical cyclogenesis occurs from a series of precursor disturbances within appropriate atmospheric environments (e.g., warm sea surface temperatures, strong divergence in upper levels, weak vertical wind shear, low-level cyclonic vorticity and moist in mid-levels; Gray, 1968; DeMaria et al., 2001; McTaggart-Cowan et al., 2013). One of these disturbances can be in the form of a tropical transition (TT; Davis and Bosart, 2004). TCs formed via TT are likely to affect Europe, since they occur in the subtropics and midlatitudes. Over the last 15 years, western Europe has been threatened by anomalous TCs that resulted from TTs, with hurricanes such as Ophelia, Leslie or Vince (Tapiador et al., 2007; Beven, 2008; Steward, 2018). Therefore, improvements in the understanding of these events could yield an important socioeconomic benefit for this region (Galarneau et al., 2015).

Tropical cyclogenesis is generally considered to occur in regions devoid of baroclinic structures; however, an appreciable number of TCs evolve in extratropical environments. McTaggart-Cowan et al. (2013) indicates that 16% of the tropical cyclogeneses recorded globally in the period 1948–2010 came from TTs, increasing this value over the North Atlantic (NATL) basin. The TT is a form of tropical cyclogenesis relatively recently described (Davis and Bosart, 2004) and associated with

extratropical precursors, i.e., is the process by which a baroclinic cyclone, with an upper-tropospheric disturbance from mid-latitudes origin, evolves and mutates into a TC. Commonly, the upper-tropospheric disturbance is forming in conjunction with Rossby waves breaking (McIntyre and Palmer, 1983; Thorncroft et al., 1993; Martius et al., 2008). These breakings can result in a variety of phenomena, namely, cutoff lows (Palmen and Newton, 1969; Nieto et al., 2005), potential vorticity (PV) streamers (Martius et al., 2008; Galarneau et al., 2015), and tropical upper-tropospheric trough cells (Sadler, 1976; Ferreira and Schubert, 1999; Patla et al., 2009). Thus, upper-tropospheric disturbances have the potential to promote TTs in environments characterized by low sea surface temperature, (SST; McTaggart-Cowan et al., 2015) and moderate-to-high vertical wind shear (Bracken and Bosart, 2000; Molinari et al., 2004; McTaggart-Cowan et al., 2008, 2013).

TTs develop more frequently in the western NATL, being less common over the eastern NATL since the environmental conditions for their formation or maintenance are marginal over the latter (Galarneau et al., 2015). TTs tend to develop in the subtropical ocean (~30°N latitude) where mid-latitude cyclones can ingest considerable moisture from the underlying ocean and tropical regions (Davis and Bosart, 2003, 2004). Compared to the western NATL at the same latitudes, SSTs over eastern NATL are lower, the vertical wind shear is higher, and, during summer, the subsidence associated to the descending branch of the Hadley circulation creates more stable and dry conditions (Hoskins et al., 2020). However, during autumn and winter these regions change their conditions and can be occasionally affected by TTs (Knapp et al., 2010).

Previous studies by Evans and Guishard (2009a), Galarneau et al. (2015), González-Alemán et al. (2015) and Bentley et al. (2017) used cyclone-relative composites to examine the upper-tropospheric features associated with NATL cyclones formation and transition processes. Both Evans and Guishard (2009b) and González-Alemán et al. (2015) suggest that the upper-tropospheric precursors to the formation of western NATL and eastern NATL subtropical cyclones differ in their structures across geopotential composites members (Figs. 7 and 5, in the respective articles). Galarneau et al. (2015) indicates that the key difference in synoptic-scale flow between developing and non-developing TC cases is the strength of the anticyclone located to the north of the incipient tropical disturbance. Bentley et al. (2017) separated subtropical cyclones that undergo a TT into three categories, based on the upper-tropospheric features associated with their formation (cutoff lows, meridional troughs, or zonal troughs) and revealed that ~61% of the subtropical cyclones form in association with an anticyclonic wave breaking.

This current study analyzes TTs over the central NATL and eastern NATL basins during the last four decades from a synoptic point of view, on a climatological basis. The main objective of this survey is to highlight the common features which lead these cyclones to evolve into TCs, with the aid of composite analysis of different fields and classifying the events according to environmental parameters. Statistical analyses to examine the TTs structure and thermodynamic differences between central NATL and eastern NATL have also been used. Additional purposes lie in analyzing the main differences between the two oceanic domains, and determining the conditions under which TTs occur in the North Atlantic. To address all these objectives, a group of TTs is built based on the Hurricane Database 2 (HURDAT; Landsea and Franklin, 2013) and specific criteria.

The organization of this paper is as follows. The datasets and the description of the methodology to identify the TTs in the HURDAT database, compute the storm-centered composites and the environmental classification are defined in Section 2. Section 3.1 explains the differences in TT density and life cycles in both domains and temporal distribution. Section 3.2 shows the storm-centered composites computed for the different dynamic fields. Section 3.3 explains the results of the environmental classification and the composites for both domains. Finally, the general conclusions are summarized in Section 4.

2. Data and methodology

2.1. Datasets used

A list of individual TTs formed over the NATL during 1979–2019 was compiled from HURDAT, identified by the National Hurricane Center. In this study, their common climatological and synoptic characteristics are studied. For this purpose, the ERA-5 climate reanalysis (Hersbach et al., 2020) is utilized. This reanalysis is generated by the European Centre for Medium-Range Weather Forecasts, being the evolution of ERA-40 (Uppala et al., 2005) and ERA-Interim (Dee et al., 2011). ERA-5 improves the spatial and temporal resolution by increasing to hourly outputs and to a 0.25° x 0.25° grid. Different studies show that ERA-5 outperforms its predecessors in many climatological applications and as an initial conditions dataset (Taszarek et al., 2020; Coffer et al., 2020; Alonso-González et al., 2021; Calvo-Sancho and Martín, 2021). A more complete explanation about ERA-5 climate reanalysis characteristics can be found in Hersbach et al. (2020).

From the ERA-5 reanalysis dataset several fields are used: geopotential height at 300 (GEO300), 500 and 1000 hPa, potential vorticity (PV) at 300 and 200 hPa, specific humidity, horizontal wind field components (u, v), potential temperature at dynamic tropopause (DT – 2 PVU, θ-DT), mean sea level pressure (MSLP) and SST. From these ERA-5 basic atmospheric fields, some derived fields are also computed: thickness between 1000 and 500 hPa (1000–500 THICK), 300–200 hPa layer averaged PV (300–200 APV), 925–500 hPa layer averaged PV (925–500 APV), equivalent potential temperature at 850 hPa (850 θ$_E$) and vertical wind shear between 850 and 300 hPa (850–300 WSH). In addition, the coupling index (CI; Bosart and Lackmann, 1995) is used. Bosart and Lackmann (1995) defined the CI as the difference between on the θ-DT and at 850 θ$_E$ and McTaggart-Cowan et al. (2015) used it to approximate the bulk column stability associated with TCs forming in the presence of an upper-tropospheric disturbance. In addition, the 1979–2019 ERA-5 climatology of every aforementioned field is computed.

Cyclones from HURDAT are selected as follow: the TCs formed from the TT process from 1979 to 2019 over the region of the North Atlantic which encompasses >60°W of longitude and > 20°N of latitude. For a TC to be considered as TT, the cyclone must transition from low, extratropical cyclone, subtropical depression or subtropical storm (LO, EX, SD or SS as named in HURDAT; Landsea and Beven, 2019) into tropical depression, tropical storm or hurricane (TD, TS or HU as named in HURDAT). An additional criterion is applied to filter out possible TCs forming from tropical easterly waves which could have been named as low and not tropical wave (WV as named in HURDAT): the TC report from the National Hurricane Center must not mention that a tropical wave intervened in the tropical cyclogenesis process. One of the TTs identified was deleted because it did not meet the minimum temporal requirement for storm-centered composite (48 h previous and 24 h after the TT). The National Hurricane Center uses the Dvorak technique for classifying the intensity of a TC (Dvorak, 1975). Although this method has elements of subjectivity, its use is supported by senior forecasters for satellite classification. Nevertheless, in the last decades, the National Hurricane Center has started to use new tools and data sources to supplement this technique, which also make this database incoherent within the selected period. For simplicity in this work any of the abovementioned tropical structures will be named as TCs.

2.2. Storm-centered composites and environmental classification methodology

Composite analyses of the 30 NATL TTs are constructed in a storm-centered relative framework for each atmospheric field used in this study. This allows us to describe the common synoptic features of the atmosphere in the proximities of the cyclones along their track. The composites are centered at the MSLP minimum, using a domain delimited by +40°/−15° in latitude and + 030°/−030° in longitude.

Timewise, the domain is centered at the time of the TT (t_0), using 24-h intervals from t_0–48 h to $t_0 + 24$ h. This grid ensures that the synoptic-scale features associated in the prior moments of the TT are adequately captured (González-Alemán et al., 2015).

A cyclone environmental classification provides us a context for TTs and, thus, gives a helpful tool to the forecasters. We based on Evans and Guishard (2009a) and González-Alemán et al. (2015) to generate the environmental classification of the chosen TTs cases. The transitions have been subdivided into four different environmental groups based upon their WSH and SST characteristics in the proximities of the cyclone. These four environments are: T (SST ≥ 25 °C, WSH ≤ 10 m s^{-1}), ST (SST ≥ 25 °C, WSH > 10 m s^{-1}), the classical extratropical type 1 (E1: SST < 25 °C, WSH >10 m s^{-1}), and the low-shear extratropical type 2 (E2: SST < 25 °C, WSH ≤ 10 m s^{-1}). Following González-Alemán et al. (2015), WSH and SST are computed using two different grids centered on the cyclone in which these two variables are averaged. The used grids comprise 3° x 3° for SST and 6° x 6° for WSH [Grid 1], and 1.5° x 1.5° for SST and 4.5° x 4.5° for WSH [Grid 2]. Additionally, an interval of uncertainty of SST and WSH using the standard deviation is introduced in the partitions of the environments for a better overview of the proximities where an extratropical or subtropical cyclone transitioned to TC.

The Mann-Whitney U test (Mann and Whitney, 1947) has been used to check statistically significant differences between the results. This test is a non-parametric test of null hypothesis: distributions of both populations are equal. With the Mann-Whitney U test, two populations are compared in order to check the independence of both groups. The p-value used is 0.05.

3. Results and discussion

3.1. Identified tropical transitions

Following the above-mentioned methodology, a set of 30 TTs within the eastern NATL and central NATL basins have been detected for the period of 1979–2019. Table 1 contains further information taken from HURDAT about the TTs identified. More than 70% of TTs transitioned from subtropical cyclones, only one transitioned from an extratropical cyclone, as classified in HURDAT and not-identified was noted for the remainder cyclones. 70% of the systems acquired tropical storm category at the moment of the TT, but only a few cyclones transitioned into tropical depression (13.3%) or into hurricane (16.7%) category. However, more than half of the storms reached the hurricane category at their maximum intensity after the TT (e.g., Ophelia, Vince or Leslie).

Fig. 1 depicts the tracks of the cyclones and their location at t_0, that is, the first moment when they were designated as TCs in the HURDAT database. Since the high density of cyclones found in the central NATL domain contrast to those noticed in the eastern NATL area, the analysis of the TTs is performed taking the two subdomains into account. Concerning the cyclone tracking, it is interesting to remark that the life cycles were longer in central NATL than in eastern NATL. Furthermore, the tropical systems cannot only organize in-situ over eastern NATL, but those which transitioned over central NATL can also enter the eastern NATL basin, driven by the westerly large-scale steering flow. This can be noted in Fig. 1 where the TT locations at different cyclone lifetimes show some systems evolving from central NATL to eastern NATL and vice versa.

The monthly TTs distribution (Fig. 2a) indicates that >70% are concentrated in autumn (September to November). This is consistent with their baroclinic origin (Davis and Bosart, 2003, 2004), as mid-latitude circulation moves southward, and thus, PV streamers and cutoff

Table 1

TTs identified from the HURDAT database during the period of 1979–2019. Domain is shown as eastern NATL (eNATL) and central NATL (cNATL). Transition time is referred as hour in UTC. The status is referred as follow: tropical depression (TD), hurricane (HU) and tropical storm (TS).

| NHC code	Storm name	Domain	Transition time (t_0)	Status	Lat (°N)	Lon (°W)	MSLP (hPa)	Wind speed (Kt)
AL141980	IVAN	eNATL	1200 1980 OCT 04	TD	36.5	023.5	1009	30
AL181980	KARL	cNATL	1800 1980 NOV 25	HU	37.7	044.7	994	65
AL201984	LILI	cNATL	1200 1984 DEC 20	HU	31.1	052.4	1002	70
AL061990	EDOUARD	eNATL	1800 1990 AUG 06	TD	37.5	033.5	1012	25
AL141990	LILI	cNATL	0000 1990 OCT 11	HU	31.2	055.9	1005	65
AL111994	FLORENCE	cNATL	1800 1994 NOV 03	TD	25.3	052.2	1005	30
AL162001	NOEL	cNATL	1200 2001 NOV 05	HU	37.8	050.3	994	65
AL172001	OLGA	cNATL	1200 2001 NOV 24	TS	29.5	049.8	1000	50
AL122002	KYLE	cNATL	0000 2002 SEP 23	TS	33.2	049.1	1009	35
AL212003	PETER	cNATL	0600 2003 DEC 09	TS	20	037.4	998	40
AL162004	OTTO	cNATL	1800 2004 NOV 30	TS	31.7	051.0	1001	40
AL242005	VINCE	eNATL	1200 2005 OCT 09	TS	33.8	019.3	1006	55
AL292005	DELTA	cNATL	1200 2005 NOV 23	TS	27.4	041.2	989	50
AL112007	JERRY	cNATL	0000 2007 SEP 24	TS	37.1	046.3	1003	35
AL122008	LAURA	cNATL	1200 2008 SEP 30	TS	40.6	048.9	1000	50
AL092009	GRACE	eNATL	0600 2009 OCT 04	TS	38.5	029.5	998	40
AL032012	CHRIS	cNATL	1200 2012 JUN 19	TS	39.4	058.7	1003	40
AL142012	NADINE	eNATL	0000 2012 SEP 23	TS	30.4	025.9	1001	45
AL192012	TONY	cNATL	1800 2012 OCT 22	TD	21.9	051.8	1006	30
AL142013	MELISSA	cNATL	0600 2013 NOV 20	TS	34.1	051.4	995	45
AL012016	ALEX	eNATL	0600 2016 JAN 14	HU	29.3	029.6	998	65
AL102016	IAN	cNATL	1200 2016 SEP 15	TS	36.3	051.5	1005	45
AL012017	ARLENE	cNATL	0000 2017 APR 20	TD	32.8	039.6	998	30
AL172017	OPHELIA	cNATL	0600 2017 OCT 09	TS	30.9	040.0	1012	35
AL042018	DEBBY	cNATL	0000 2018 AUG 08	TS	39.7	049.2	1010	35
AL052018	ERNESTO	cNATL	1800 2018 AUG 16	TS	42.4	042.1	1007	40
AL102018	JOYCE	cNATL	0000 2018 SEP 14	TS	33.1	044.4	1006	35
AL132018	LESLIE	cNATL	1800 2018 SEP 29	TS	34.3	051.3	994	45
AL162018	OSCAR	cNATL	1800 2018 OCT 27	TS	27.1	049.9	1005	50
AL182019	PABLO	eNATL	1800 2019 OCT 25	TS	35.9	032.7	995	40
Avg			15 SEP		33.2	043.4	1002.0	44.2
Std dev			8.76 days		05.4	010.3	5.9	12.2

Tropical Transitions Tracks | X - Tropical Transition
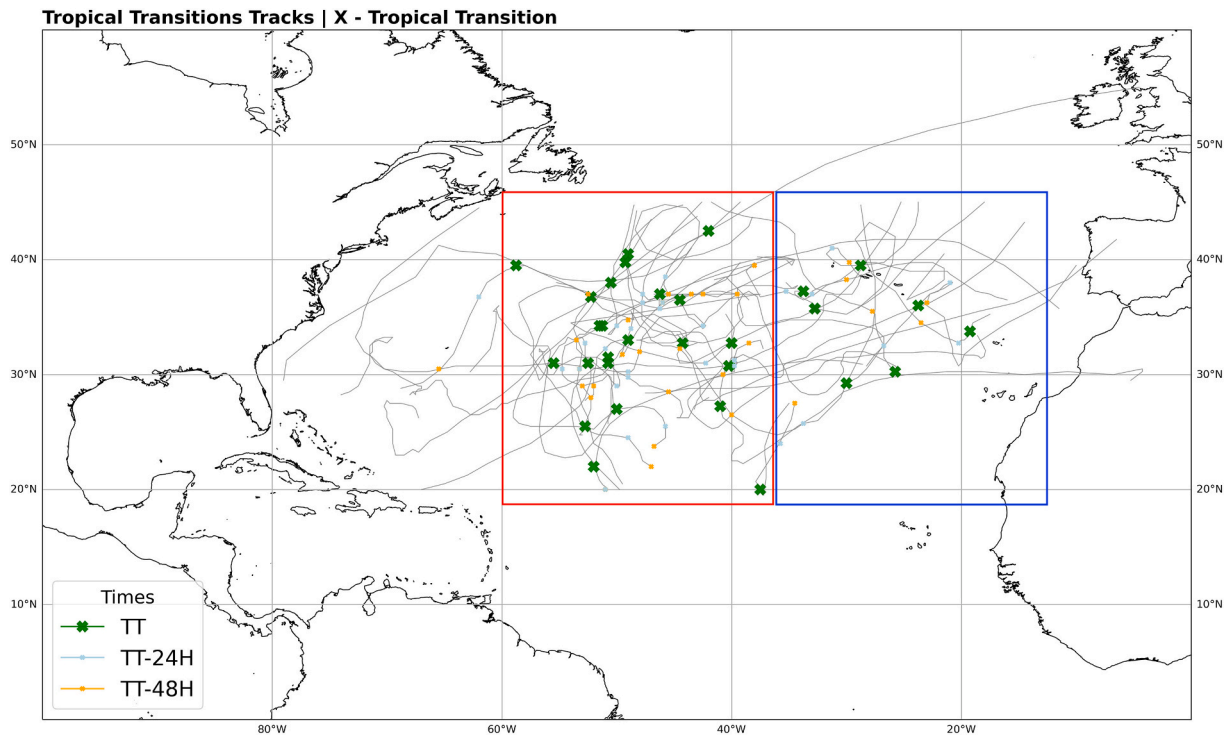
Fig. 1. Tracks of the identified cyclones that transitioned into a TC within NATL during the period 1979–2019. The crosses indicate the position of the cyclones at the time of the transition (t_0). The red domain is for central NATL and the blue domain is for eastern NATL.

lows are more frequent over the region due to the increase of baroclinicity. Although there is some TTs in spring and December, the TTs for the central NATL domain mainly cover autumn, with peaks from September to November. This might be linked with the high activity in these months of PV streamers (Papin et al., 2020) and tropical upper-tropospheric troughs (Sadler, 1976). PV streamers climatology shows higher occurrence frequency over central NATL from July to October (Papin et al., 2020), while the peak activity of tropical upper-tropospheric troughs is September and concentrated between 030°-040°N and 040°-060°W (Postel and Hitchman, 1999). The weakening of the subtropical anticyclonic ridge, and an increase of cut-off lows overlapping with relatively warm SSTs reaching their northernmost extent (Font, 1983), might be behind the maximum activity of TTs found for the eastern NATL domain in October. Furthermore, this eastern NATL maximum activity in autumn can also be linked to a negative North Atlantic Oscillation (NAO) since its minimum phase is recorded in October, as per the monthly averages computed (not shown). On the other hand, TTs frequency show secondary minimum values in winter. In these months, latent heat release is not so prevalent as in the autumn, so convection does not play that relevant role to promote TTs.

79% of the total TTs have been recorded in the current century, and more precisely, 48% of all TTs have been recorded in the last decade (Fig. 2b). Even if HURDAT is a subjective database which may not be completely coherent during the whole period, the results show that the number of TTs has greatly increased. This could be partially related to results obtained by Muñoz et al. (2020), who indicate an increase of cut-off lows over the North Hemisphere in the last 70 years. Furthermore, TTs have an important contribution for the annual tropical cyclone genesis frequency (shown in supplementary material S1). As an example, 33.3% of tropical cyclones were generated by a TT in 2018.

3.2. Storm-centered composites

Composites of several basic and derived atmospheric fields are analyzed in this section to describe the common synoptic features of the

cyclones evolving into a TC in the North Atlantic basin. Composites of GEO300, MSLP, 1000–500 THICK, 850 θ_E, 300–200 APV, 925–500 APV, 850–300 WSH, θ-DT and CI are computed as well as the anomaly composites to show more detailed environmental features.

A westerlies meridional trough promotes a low-pressure system at surface via quasigeostrophic forcing, just to the south of the trough's axis. This becomes the dominant feature prior to the transition into TC (Fig. 3a, b). In addition, the TTs are characterized by a strong anticyclone to the north-northeast of the surface cyclone (Fig. 3c), which provides moisture to the cyclone by the enhanced surface latent heat fluxes in the regions of strong pressure gradient (Galarneau et al., 2015). In almost every TT case, a trough was likewise visible close to the surface low while not all the troughs were in the same state of evolution at t_0–24. As time passes, the trough at 300 hPa and the 1000–500 THICK evolve to increase the geopotential height (Fig. 3c, d, g, h), which could indicate a warm core transition. Nevertheless, a remarkable deepening of MSLP cannot be observed. This could be because the cyclones begin to be governed by diabatic processes when they transition, which cannot be properly represented in ERA5 because of its spatial resolution (Bolgiani et al., 2022). This weak MSLP deepening can be indeed related to the convective activity via greater diabatic heating forcing associated with its latent heat release (shown in supplementary material S2). This diabatic heating forcing can be seen in the convective precipitation field, which displays an increase of convective activity just below the upper-level disturbance (shown in supplementary material S3). Therefore, the cyclone adopts a more tropical structure (Fig. 3d, h).

The diabatic heating forcing can be explained in terms of the Lagrangian tendency of potential vorticity (PV) due to a diabatic heat source represented by (Hoskins et al., 1985).

$$\rho \frac{dPV}{dt} = \eta_a \cdot \nabla \dot{\theta}$$

where ρ is the atmospheric density, η_a is the three-dimensional absolute vorticity vector, and $\dot{\theta}$ is the diabatic heating rate (i.e., $d\theta/dt$). The PV can be redistributed vertically by introducing a differential diabatic heat
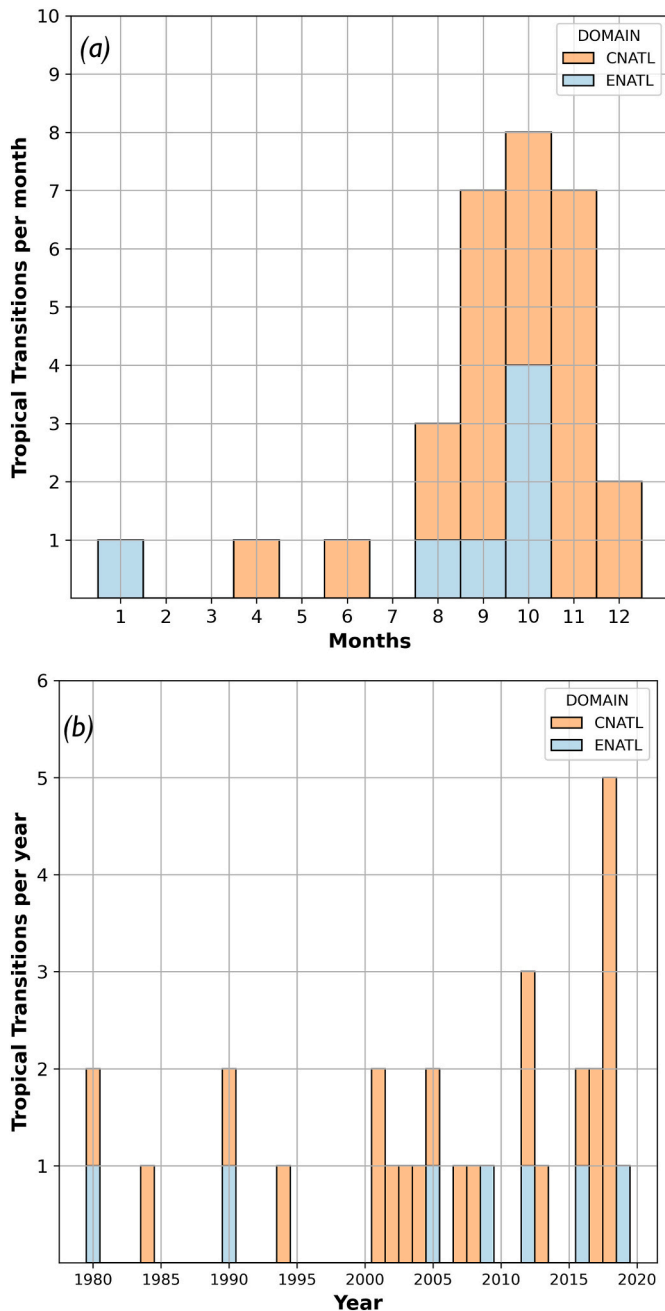
Fig. 2. (a) Monthly and (b) yearly distribution of the TTs identified within the NATL basin during the period 1979–2019.

source (e.g., latent heat release) into the column. Assuming that the diabatic heating maximum is situated in the mid-troposphere and the absolute vorticity vector is nearly vertical, PV will tend to increase (decrease) in the layer below (above) the heating maximum. This heating will therefore be reflected as an anomalously high PV in the lower troposphere with lower values near the tropopause, which is in line with Hulme and Martin (2009), who state that in the moments previous to the TT large releases of latent heat promote a low-level increase of PV and intensifies the circulation around the cyclone center in the lower troposphere. As it can be seen in Fig. 4, the PV decreases in the upper troposphere as the moment of TT approaches (Fig. 4b, c) while in the lower troposphere the values are increasing (Fig. 4f, g). However, it is practically constant after t_0 when the system is already a tropical cyclone.

In the composite results, there is an apparent inconsistency in the

mechanism associated with the Lagrangian tendency of PV, as the decrease in higher levels is not matched by the behavior in lower levels after the TT. The low-level PV behavior can be explained by the non-advective PV tendency that considers the three-dimensional gradient of the diabatic heating due to latent heat release (Cammas et al., 1994; Emanuel, 1986; Hulme and Martin, 2009). As it is abovementioned, if there is a heating maximum in the middle troposphere levels and an upward-directed absolute vorticity vector, this maximum will be reinforced (weaken) by PV in low (upper) levels (Raymond, 1992). To illustrate this result, the non-advective PV tendency is derived for all the selected TTs (not shown). While the non-advective PV tendency values are increasing from t_0–48h to t_0 in low levels (900–800 hPa) around the surface cyclone, the values are reducing in upper-levels (200–300 hPa). From t_0, the non-advective PV tends to vanish in low-levels and upper-levels, being consistent with the redistribution of the potential vorticity. Analyzing each result of every TT, the role of the latent heat release in this kind of systems and their transitions, and its influence over the non-advective PV, is highlighted. The derived composites of the non-advective PV tendency (shown in the supplementary material S4) verify increases (decreases) of PV throughout the evaluated period in low (upper) levels. The averaged PV vertical profile obtained in 300 km-radius around the cyclone center (shown in the supplementary material S5) also depicts a PV increase (decrease) at low (upper) levels throughout the life cycle of the TTs.

Fig. 4 shows how the APV in 300–200 hPa (900–800 hPa) depicts decreasing (increasing) values from t_0–48 h to t_0. The quasi-constant APV values in 900–800 hPa from t_0 are related to the sustained non-advective PV tendency. In fact, the evolution of averaged non-advective PV tendency in a radius of 300 km centered in the cyclones displays values of $1.5 \times 10^{-6}\,\mathrm{K\,h^{-1}}$ (t_0–48 h), $1.0 \times 10^{-6}\,\mathrm{K\,h^{-1}}$ (t_0–24 h), $0.4 \times 10^{-6}\,\mathrm{K\,h^{-1}}$ (t_0 h) and $0.4 \times 10^{-6}\,\mathrm{K\,h^{-1}}$ ($t_0 + 24$ h). The differences between individual TT results of APV (not shown), with more clear and noticeable latent heat release effect, and the composite APV results (Fig. 4) are promoted by the averaged values of various vertical levels for several TTs, blurring, in some way, the individual results.

The 850–300 WSH composite (Fig. 5) shows a decrease in the environmental wind shear due to the occlusion process of the extratropical cyclone, which indicates a transition into a barotropic environment as expected in a TT process (Davis and Bosart, 2004). Wind shear is consequently reduced by vertical redistribution of PV due to the abovementioned differential diabatic heating.

Contrary to the historic reasoning, TCs evolving from TTs have the potential to form over SSTs <26.5 °C in environments characterized by notably reduced stability (Mauk and Hobgood, 2012; McTaggart-Cowan et al., 2015). This reduction of bulk column stability over 'low' SSTs is typically associated with the presence of an upper-tropospheric disturbance that lowers the DT height, steepening environmental lapse rates and facilitating the development of deep convection that serves as a catalyst. The θ-DT field shows a decrease of DT height, which fosters deep convection (Fig. 6a, b, c). The slight rise in θ-DT values over the cyclone center after the transition moment (Fig. 6d), corresponding to an approximate reduction of 0.5 PVU in the 300–200 APV values over the cyclone center (Fig. 4d), indicates that the upper-tropospheric disturbance is being dissipated by the diabatic vertical redistribution.

The CI composite shows a reduction which indicates enough environmental instability for TT (Fig. 6e, f, g, h). McTaggart-Cowan et al. (2015) suggest a CI global value of 22.5 °C as the upper limit for TTs developments. This reduction of tropospheric stability facilitates the development of the deep convection which feeds the cyclone and allows it to accomplish the TT. The increase of instability (reduced CI) in the previous stages to the TT is coherent with the deepening of the upper-tropospheric precursor (Fig. 6b, c) and the increase in low-level θ_E, being this increase related to enhanced surface latent heat fluxes and more intense than the deepening of θ-DT values.
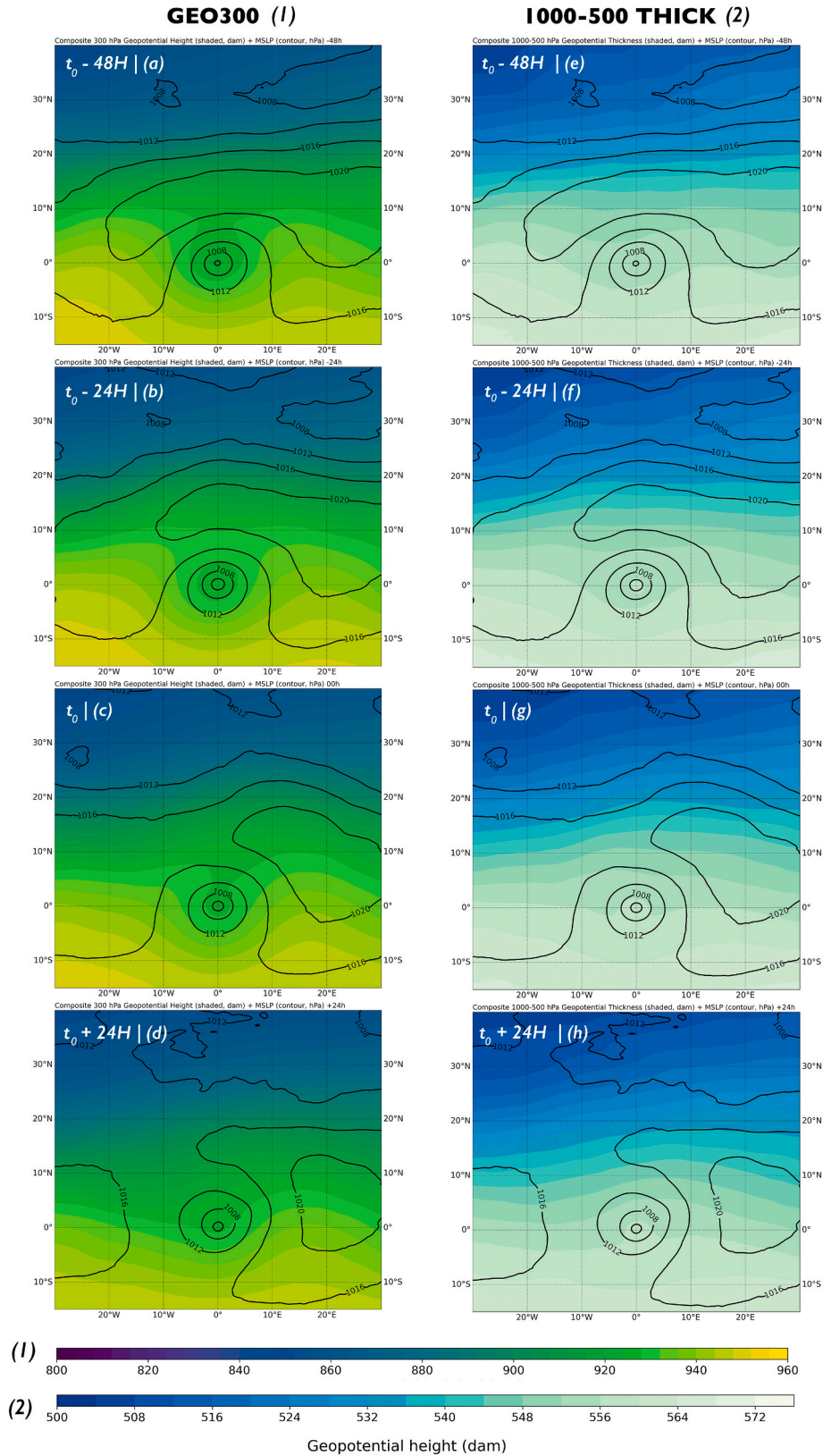
NORTH ATLANTIC BASIN

GEO300 *(1)*   ### 1000-500 THICK *(2)*

Fig. 3. Storm-centered composited for the 33 TTs evaluated in NATL. (a) t_0–48 h, (b) t_0–24 h, (c) t_0, (d) t_0 + 24 h of GEO300 (shaded, dam) and MSLP (black contours, hPa); (e) t_0–48 h, (f) t_0–24 h, (g) t_0, (h) t_0 + 24 h of 1000–500 THICK (shaded, dam) and MSLP (black contours, hPa).

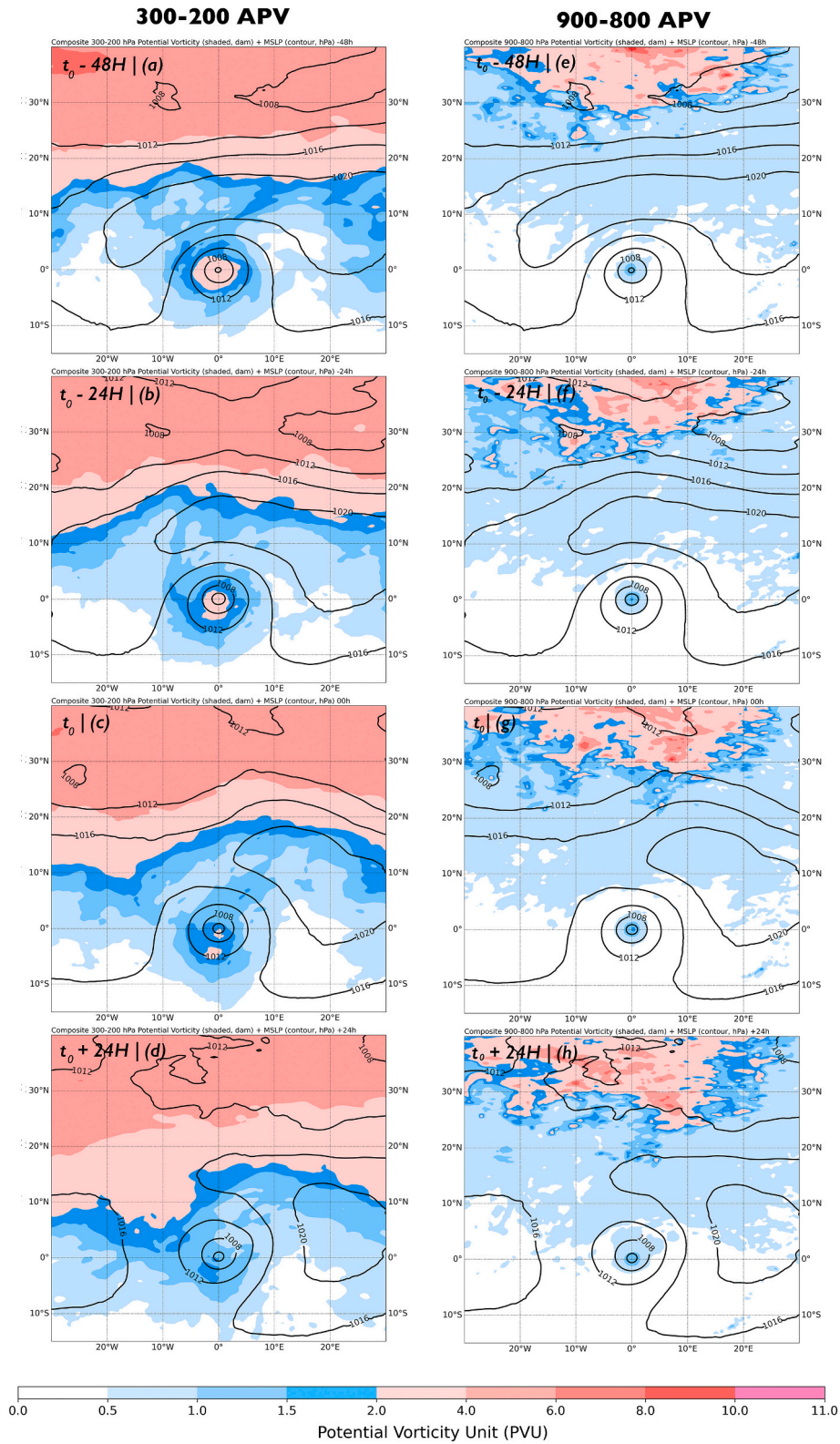**Fig. 4.** As in Fig. 3, except for (a), (b), (c) and (d) 300–200 hPa APV (shaded, PVU) and MSLP (black contours, hPa); (e), (f), (g) and (h) 900–800 hPa APV (shaded, PVU) and MSLP (black contours, hPa).

North Atlantic Basin

850-300 WSH
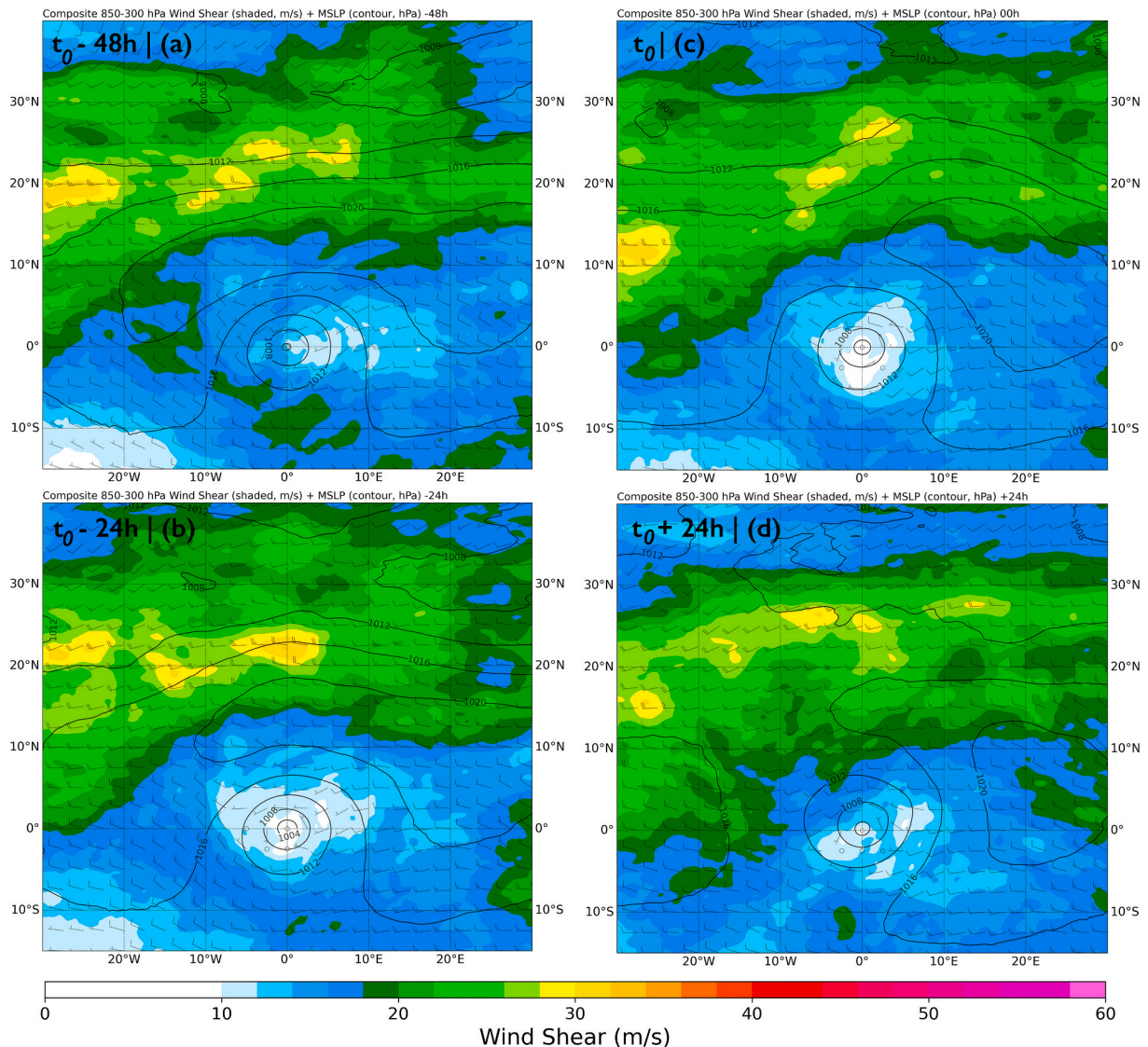
Fig. 5. As in Fig. 3, except for (a), (b), (c) and (d) 850–300 hPa WSH (shaded, m s-1) and MSLP (black contours, hPa).

3.3. Environmental classification

An environmental classification of the identified TTs is undertaken in this section. As mentioned in Section 2.3, the TTs have been subdivided into four different environments (tropical, subtropical, E1 and E2) based upon their WSH and SST environmental values around the cyclone, from t_0–48 h to t_0 + 24 h. These two atmospheric variables used to retrieve the classification of the TT environments are linked with processes involved in the development of cyclones. The proportion between these processes plays an influential role in determining the final cyclone structure (Davis and Bosart, 2003, 2004). As it is abovementioned, two grids are used to locate a TT in its corresponding environmental group. Both WSH and SST are derived by taking the variable averaged in the corresponding grid centered on the cyclone. Although SST values show more similarity in both grids (mean SST1 = 23.8, mean SST2 = 22.5 corresponding to Grid 1 and Grid 2, respectively), the WSH show lower values in Grid 2 than in Grid 1 (mean WSH1 = 11.3, mean WSH2 = 9.4). González-Alemán et al. (2015) highlight, using similar grids, lack of

sensitivity in the SST to changes in the size of the grid box with no significant differences, and significant ones in WSH. Here, there is some sensitivity of the SST to changes in the domain grid resolution and WSH shows more sensitive to them. Small differences are found in SST and WSH when Grid 1 and Grid 2 are used except for some TTs located in different extratropical environment of formation associated to different WSH but with similar SST. Thus, it is necessary to take an uncertainty interval into account (Fig. 7). As few studies consider this kind of methodology at knowledge of the authors (Evans and Guishard, 2009b; González-Alemán et al., 2015), to contrast the results with such studies and for a better representation of the cyclone structures, the Grid 1 has been finally chosen.

The tropical environment most prone to cyclogenesis is the tropical group, characterized by low WSH and warm SST. The ST environment shares warm SSTs with the T environment, which contributes with near-surface thermodynamic forcing via moisture and sensible fluxes. Nonetheless, the ST environment is characterized by a strong WSH, i.e., more favorable for baroclinic development. In contrast, the extratropical
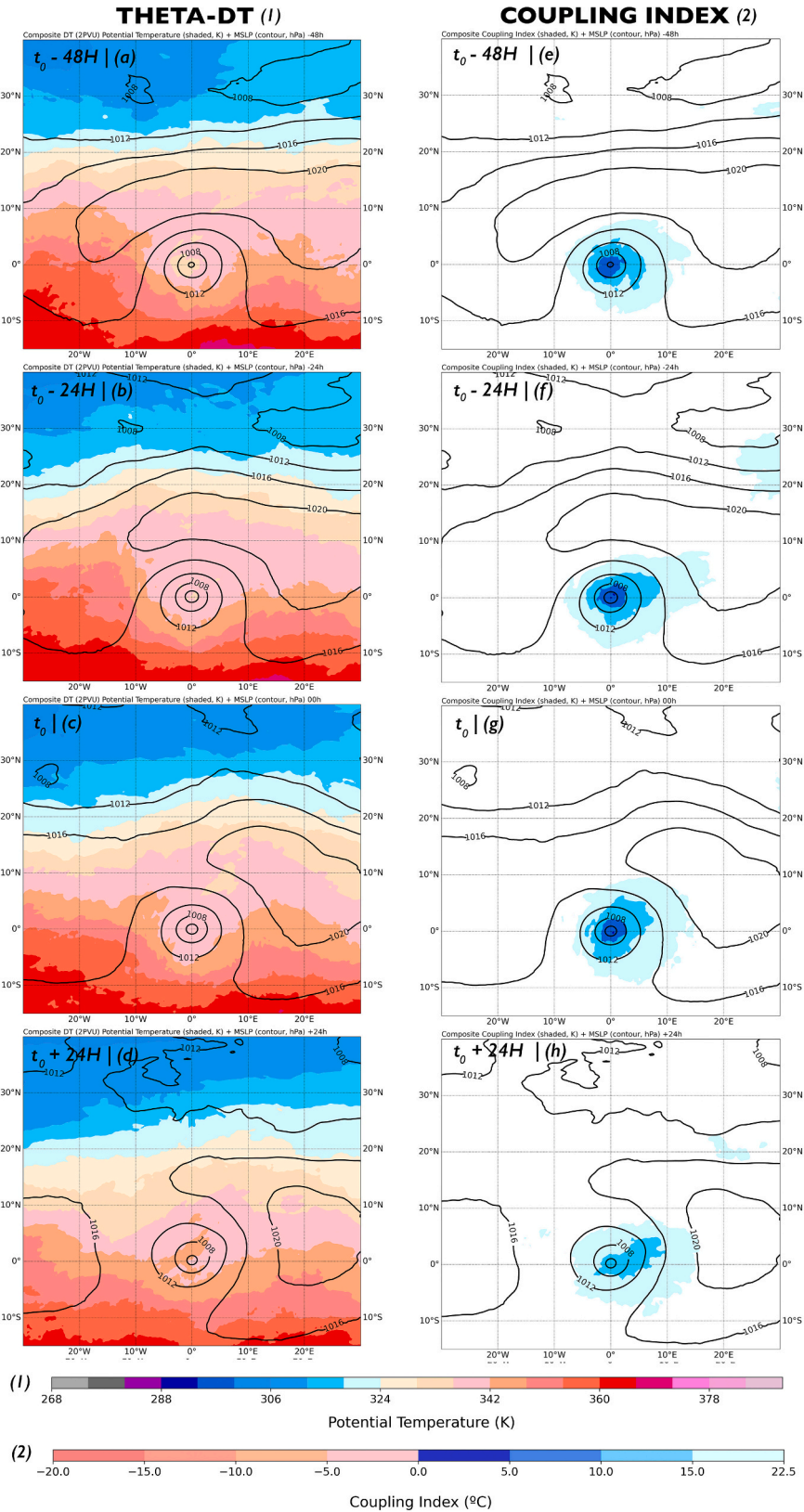
NORTH ATLANTIC BASIN

Fig. 6. As in Fig. 3, except for for (a), (b), (c) and (d) θ-DT (shaded, PVU) and MSLP (black contours, hPa); (e), (f), (g) and (h) CI (shaded, PVU) and MSLP (black contours, hPa).
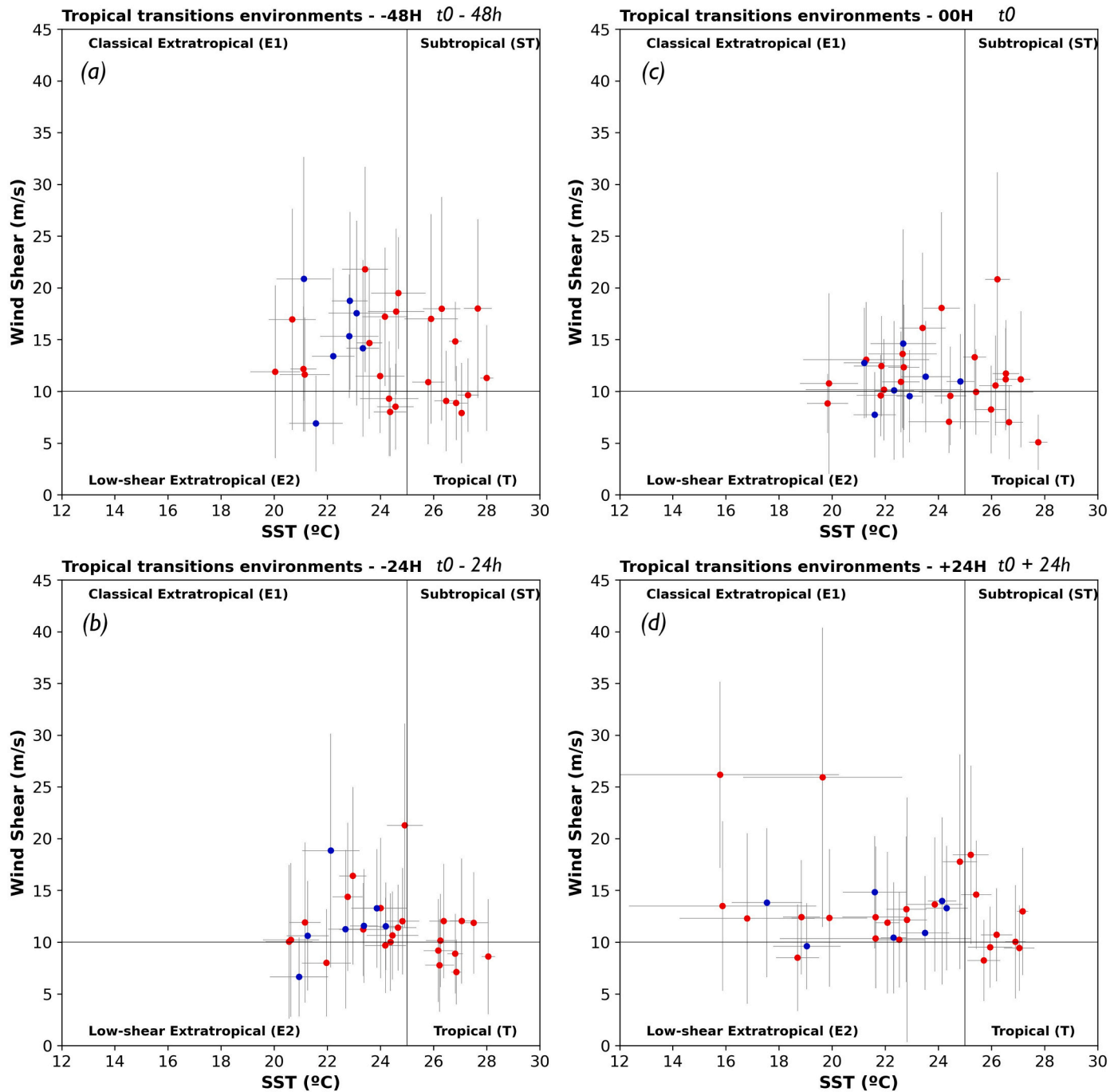
Fig. 7. Partition of the 33 TT cases based upon characteristics of their synoptic environment at (a) t_0–48, (b) t_0–24, (c) t_0 and (d) $t_0 + 24$. Red dots: central NATL; blue dots: eastern NATL. Grid 1 used. Uncertainty bars indicate the standard deviation.

environments (E1 and E2) are characterized by cooler SSTs. Thus, the presence of an upper-level trough will more likely force a baroclinic cyclone development. However, the E2 environment is characterized by weak WSH, which may enable the convective activity to be maintained if developed, because of instability, and favors the accumulation of the latent heat released. This accumulation of heating could produce a warm core thermal structure in the lower and middle (upper) levels of the troposphere, which is characteristic of subtropical cyclones (TC) structures.

The diagrams of Fig. 7 depict a predominance of extratropical environment instead of tropical/subtropical environment (66.7% and 33.3%, respectively) at t_0 (Fig. 7c). It is remarkable that >50% of the cyclones transitioned into TC in extratropical environments,

characterized by cold SSTs and relatively high WSH. However, between t_0–48h and t_0 -24h, 78.7% of the cyclones present reduced WSH and 45% increased SST (Fig. 7a, b). This reduction in WSH and increase in the SST favors the convective activity and the warm core development via the accumulation of latent heat release.

The differences between central NATL and eastern NATL are remarkable. Cyclones in central NATL transitioned into TC predominantly in E1 environments (39.1%), while 26.1% and 17.4% of the cyclones transitioned in tropical and subtropical environments, respectively. In other words, 50% of the cyclones transitioned in environments with cooler SSTs and low/medium WSH. On the other hand, cyclones in eastern NATL transitioned predominantly in E1 (71.4%) and E2 (28.6%) environments. However, no cyclones have undergone TT in

tropical environment in eastern NATL. Thus, the central NATL shows a more tropical environment while the eastern NATL exhibits an extratropical environment when cyclones transitioned. The obtained results for both WSH and SST between central NATL and eastern NATL are statistically significant at 95% level (p-value 0.025 and 0.0001, respectively).

Evans and Guishard (2009a) identified 18 subtropical cyclones in western NATL, formed predominantly in subtropical and tropical environments, each representing 38.9% (7 cyclones) of the total. However, only one and three cyclones formed under E1 and E2 environments, respectively. These results contrast with González-Alemán et al. (2015), whose results show that all subtropical cyclones formed within the eastern NATL basin did in extratropical environments (71.4% E1 and 28.6% E2). Although these distinctions between the western NATL and eastern NATL domains are related only to subtropical cyclones, they are consistent with our results, revealing more extratropical genetic environments in eastern NATL and more tropical environments in central NATL.

The statistically significant differences obtained in the environmental classification between the central NATL and eastern NATL basins instigates us to further analyze their atmospheric conditions. Storm-centered composites for different cyclones developed in each basin are next examined for possible synoptic features differences.

3.4. Storm-centered composites – central NATL vs. eastern NATL basin

Comparing the environment at the eastern NATL basin against central NATL, the GEO300 field displays a deeper trough, a stronger anticyclone north of the surface cyclone (Fig. 8a, b, c, d) and a lower 1000–500 THICK (Fig. 8e, f, g, h). The GEO300 field for the central NATL basin displays a quasi-isolated upper-tropospheric disturbance, while for eastern NATL the disturbance is more connected to the westerly circulation. For central NATL, the synoptic environment favors the transition with a more robust warm core (isohypses are shifted northward) while for eastern NATL they transition in environments with enhanced surface latent heat fluxes (shown in supplementary material S6). The MSLP field shows a deep low just below the upper-level disturbance for eastern NATL at t_0–24 h, however it is not deepening at t_0. In contrast, the central NATL cyclones evolve into a deeper pressure system at t_0.

From a 300–200 APV perspective, there are remarkable differences between eastern NATL and central NATL (Fig. 9a, b, c, d). For the eastern NATL basin, the upper-tropospheric PV values in the center and in the proximities of the cyclone are higher than for the central NATL basin, which indicates a deeper upper-level disturbance, consistent with the GEO300 field (Fig. 8). The CI field reveals higher instability for eastern NATL than for central NATL at t_0–24 and t_0 (Fig. 9c, d, e, f). This is associated with higher values of θ-DT in central NATL than in eastern NATL (shown in supplementary material S7), i.e., the upper-tropospheric disturbance influences more in the CI than the low-levels moisture advection. In fact, the θ-DT values for eastern NATL are lower than for central NATL, indicating that the upper-tropospheric disturbance is promoting lower heights of DT (shown in supplementary material S7). Therefore, the decrease of the bulk column stability, as noted by the CI, favors the development of deep convection, which in turn promotes TTs even over lower SSTs, as is the case for eastern NATL. In other words, instability seems to play more notable role for eastern NATL transitions than for central NATL ones.

Unlike the eastern NATL cyclones, the central NATL cyclones transition in environments characterized by low vertical WSH (< 10 m s^{-1}; Fig. 10a, b, c, d), possibly due to more barotropic environments, related to broader regions of warmer SSTs and lower horizontal thermal gradients (not shown). The cyclones in the eastern NATL basin are associated with moderate WSH environments at t_0–24 h, highlighting a decrease of WSH at t_0. This is because eastern NATL transitions are characterized by a more extratropical environment, i.e., more

baroclinicity than for central NATL. The moderate WSH values are also associated with higher PV gradients for eastern NATL when compared to central NATL (Fig. 9a, c).

Once the system is a TC ($t_0 + 24$), differences for both basins are maintained, which can be also seen in additional fields. Outgoing longwave radiation composites for central NATL exhibit widespread lower values surrounding the cyclone (not shown) in comparison with the eastern NATL ones. Moreover, the total column water (Fig. 10e, f, g, h) and 850 θ$_E$ fields also show higher values in wider areas for central NATL cyclones than for eastern NATL ones. All these features make central NATL TT-generated TCs to be more robust and bigger than in eastern NATL, as noted by an inspection of satellite images (not shown). This is also confirmed by a more symmetrical and deeper MSLP field in central NATL TCs.

4. Summary and conclusions

This study develops a climatology of TTs in the North Atlantic basin and analyzes the synoptic and environmental features during the 1979–2019 period using ERA-5 reanalysis data. TTs are identified in the HURDAT database through cyclones in baroclinic structures transitioned to TC. Subtropical cyclones are the most likely cyclonic structure to transition to TC, having made up 70% of all TTs. At the TT time almost all TTs had tropical storm category, albeit more than half of the TTs evolving to hurricane in their maximum intensity. The highest density and longest life cycles of TTs in North Atlantic begin in central NATL basin; however, the TTs transitioned over the central NATL can enter into the eastern NATL basin driven by the westerlies flow. The central NATL basin maximum is in autumn, linked with the warmer SSTs and might be related with tropical upper-tropospheric trough cells. The eastern NATL basin maximum activity is in October, linked with the warmer SSTs that reach their northernmost extend, as well as an increasingly frequent of cutoff lows, causing the region to become favorable for deep convection development. TT is favored in environments that overlaps a baroclinic zone with warmer SSTs.

The storm-centered composite maps reveal a strong anticyclone northern to the surface cyclone and the trough at GEO300 and 1000–500 THICK, which evolves into a warm core through an increase in the geopotential height. The reduction of tropospheric stability, displayed in the CI field, in the previous moments to the TT time indicates enough thermal instability for TT to occur and facilitates the development of deep convection. Deep convection favors latent heat release which promotes the vertical redistribution of the PV, with a drop (increase) aloft (low levels) of PV values at the time of TT and a reduction of the 850–300 WSH, which confirms the transition to a more barotropic environment.

The environmental classification showed that there is a predominance of extratropical instead of tropical/subtropical environment (66.7% and 33.3%, respectively); however, >50% of the cyclones transitioned to TC in non-tropical environments. The differences between central NATL and eastern NATL are remarkable: 43.5% of the central NATL cyclones transitioned in environments characterized by warm SSTs and low-to-moderate WSH, while >70% of eastern NATL cyclones transitioned in environments characterized by cold SSTs and moderate-to-high WSH. Therefore, the central NATL TTs show a more tropical environment.

The storm-centered composite maps differences between central NATL and eastern NATL were prompted by the statistically significant differences found in the environmental classification. The composite maps reveal important and statistically significant spatial differences comparing both basins. The eastern NATL cyclones transitioned in environments with high 300–200 PV and CI values, and enhanced surface latent heat fluxes, while central NATL cyclones transitioned in a more barotropic environment characterized by low 850 WSH and warm SSTs. The most remarkable synoptic environment difference between both basins lies in the higher PV values at upper levels, which can be located
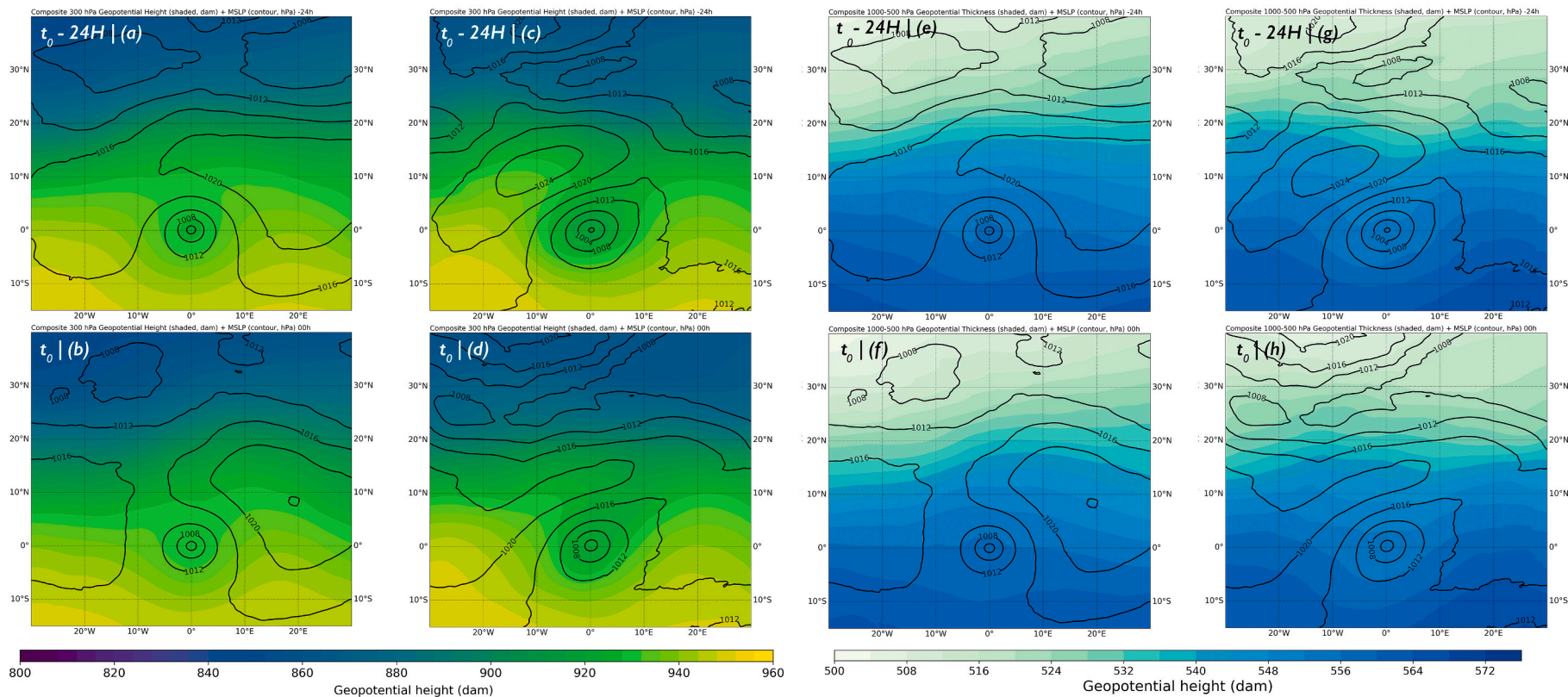
GEO300

1000-500 THICK

Fig. 8. Storm-centered composites for the central NATL and eastern NATL basins (a, c) t_0–24 h, (b, d) t_0 of GEO300 (shaded, dam) and MSLP (black contours, hPa); (e, f) t_0–24 h, (g, h) t_0 of 1000–500 THICK (shaded, dam) and MSLP (black contours, hPa).
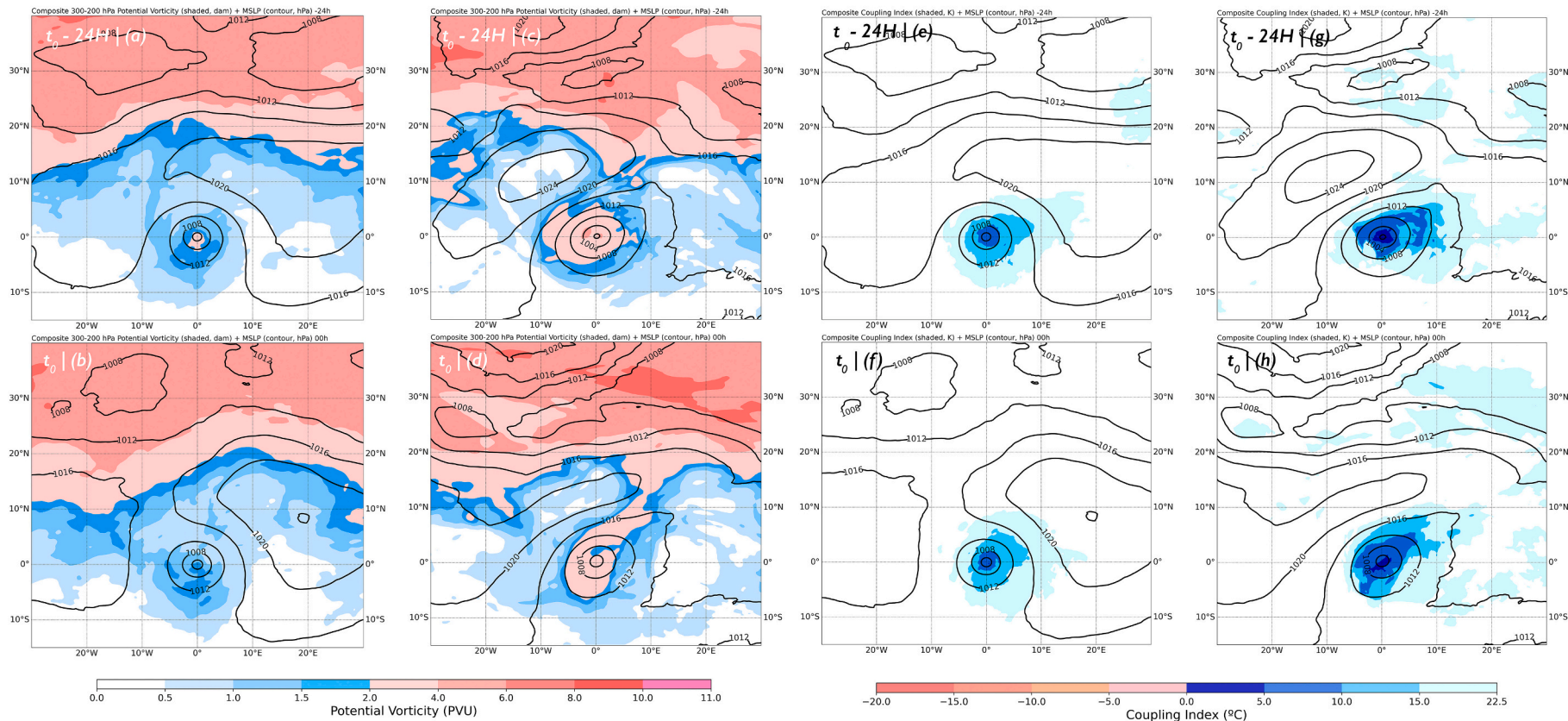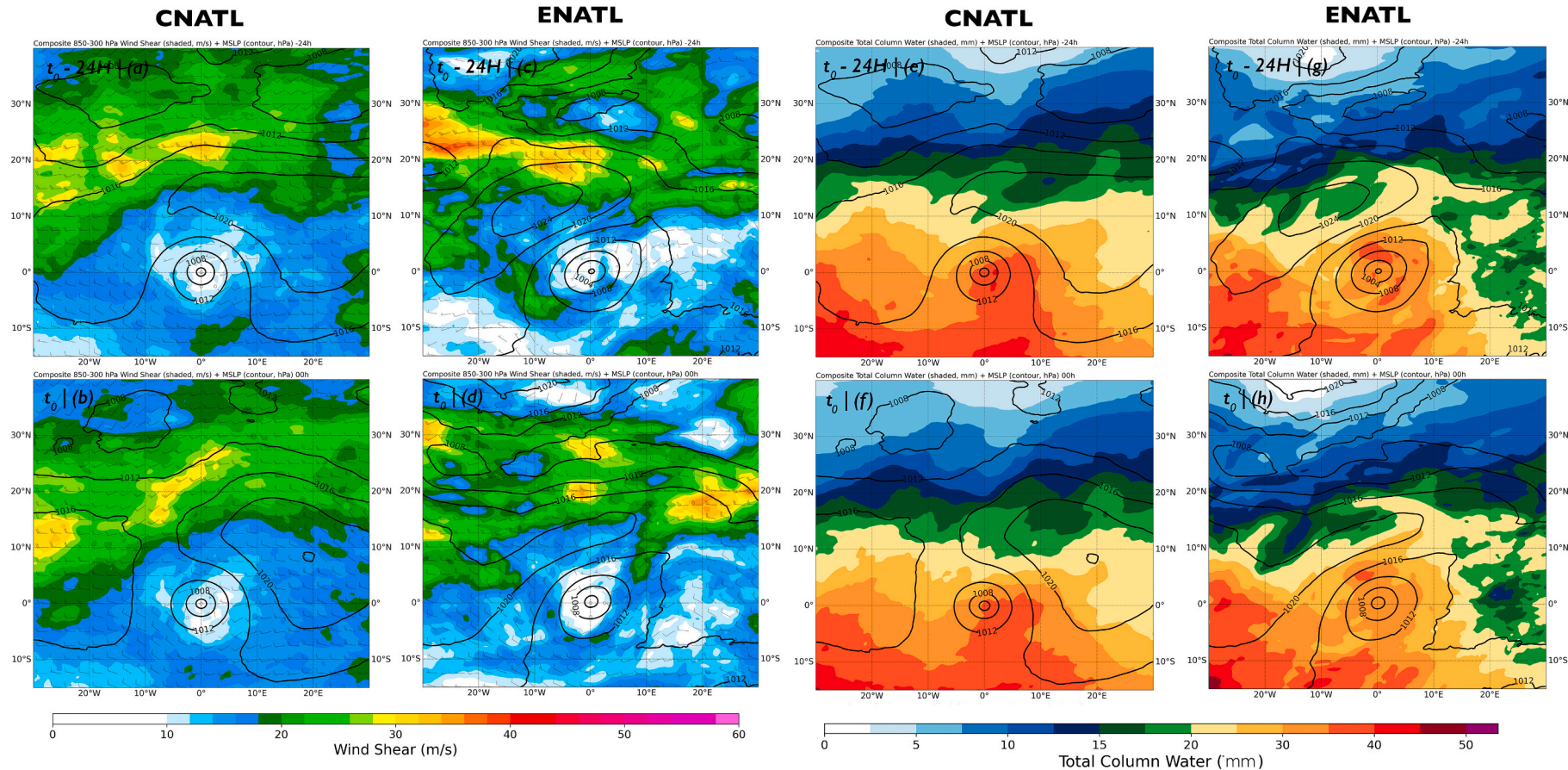
300-200 APV

COUPLING INDEX

Fig. 9. As in Fig. 8, except for for (a), (b), (c) and (d) 300–200 APV (shaded, PVU) and MSLP (black contours, hPa); (e), (f), (g) and (h) CI (shaded, PVU) and MSLP (black contours, hPa).

850-300 WSH

TOTAL COLUMN WATER

Fig. 10. As in Fig. 8, except for for (a), (b), (c) and (d) 850–300 WSH (shaded, PVU) and MSLP (black contours, hPa); (e), (f), (g) and (h) total column water (shaded, PVU) and MSLP (black contours, hPa).

in the center of the cyclone for eastern NATL. These differences make central NATL TCs show a more tropical and robust structure than in eastern NATL.

The analysis presented here has pointed to the importance of the environmental and dynamical synoptic distributions in numerous TTs events. Although ERA-5 resolution improves old reanalysis, more research is needed in high-resolution models, allowing the study of the interactions between large-scale and convection processes in the TTs.

CRediT authorship contribution statement

C. Calvo-Sancho: Conceptualization, Methodology, Software, Formal analysis, Writing – original draft. **J.J. González-Alemán:** Conceptualization, Methodology, Formal analysis. **P. Bolgiani:** Supervision. **D. Santos-Muñoz:** Supervision. **J.I. Farrán:** Software. **M.L. Martín:** Conceptualization, Methodology, Writing – review & editing, Supervision, Funding acquisition.

Declaration of Competing Interest

The authors declare no conflicts of interest regarding the publication of this paper.

Acknowledgements

Appendix A. Supplementary data

Supplementary data to this article can be found online at https://doi.org/10.1016/j.atmosres.2022.106353.

References

Alonso-González, E., Gutmann, E., Aalstad, K., Fayad, A., Bouchet, M., Gascoin, S., 2021. Snowpack dynamics in the Lebanese mountains from quasi-dynamically downscaled ERA5 reanalysis updated by assimilating remotely sensed fractional snow-covered area. Hydrol. Earth Syst. Sci. 25, 4455–4471. https://doi.org/10.5194/hess-25-4455-2021.

Bentley, A.M., Bosart, L.F., Keyser, D., 2017. Upper-tropospheric precursors to the formation of subtropical cyclones that undergo tropical transition in the North Atlantic Basin. Mon. Weather Rev. 145, 503–520. https://doi.org/10.1175/MWR-D-16-0263.1.

Beven, J.L., et al., 2008. Atlantic hurricane season of 2005. Mon. Wea. Rev 139, 1109–1173.

Bolgiani, P., Calvo-Sancho, C., Díaz-Fernández, J., Quitián-Hernández, L., Sastre, M., Santos-Muñoz, D., Farrán, J.I., González-Alemán, J.J., Valero, F., Martín, M.L., 2022. Wind kinetic energy climatology and effective resolution for the ERA5 reanalysis. Clim. Dyn. https://doi.org/10.1007/s00382-022-06154-y.

Bosart, L.F., Lackmann, G.M., 1995. Postlandfall tropical cyclone reintensification in a weakly baroclinic environment: a case study of hurricane David (September 1979). Mon. Weather Rev. 123, 3268–3291. https://doi.org/10.1175/1520-0493(1995)123<3268:PTCRIA>2.0.CO;2.

Bracken, W.E., Bosart, L.F., 2000. The role of synoptic-scale flow during tropical cyclogenesis over the North Atlantic Ocean. Mon. Weather Rev. 128, 353. https://doi.org/10.1175/1520-0493(2000)128<0353:TROSSF>2.0.CO;2.

Calvo-Sancho, C., Martín, Y., 2021. Supercell Pre-convective Environments in Spain: a dynamic downscaling of ERA-5 Reanalysis, EGU General Assembly 2021, online, 19–30 Apr 2021, EGU21-2967. https://doi.org/10.5194/egusphere-egu21-2967.

Cammas, J.-P., Keyser, D., Lackmann, G.M., Molinari, J., 1994. Diabatic redistribution of potential vorticity accompanying the development of an outflow jet within a strong extratropical cyclone. In: Preprints, Int. Symposium on the Life Cycles of Extratropical Cyclones, Vol. II. Bergen. Geophysical Institute, University of Bergen, Norway, pp. 403–409.

Coffer, B.E., Taszarek, M., Parker, M.D., 2020. Near-ground wind profiles of tornadic and nontornadic environments in the United States and Europe from ERA5 reanalyses. Weather Forecast. 35, 2621–2638. https://doi.org/10.1175/WAF-D-20-0153.1.

Davis, C.A., Bosart, L.F., 2003. Baroclinically induced tropical cyclogenesis. Mon. Weather Rev. 131, 2730–2747. https://doi.org/10.1175/1520-0493(2003)131<2730:BITC>2.0.CO;2.

Davis, C.A., Bosart, L.F., 2004. The TT problem: forecasting the tropical transition of cyclones. BAMS. 85 (11), 1657–1662. https://doi.org/10.1175/BAMS-85-11-1657.

Dee, D.P., Uppala, S.M., Simmons, A.J., Berrisford, P., Poli, P., Kobayashi, S., Andrae, U., Balmaseda, M.A., Balsamo, G., Bauer, P., Bechtold, P., Beljaars, A.C.M., van de Berg, L., Bidlot, J., Bormann, N., Delsol, C., Dragani, R., Fuentes, M., Geer, A.J., Haimberger, L., Healy, S.B., Hersbach, H., Hólm, E.V., Isaksen, L., Kållberg, P., Köhler, M., Matricardi, M., McNally, A.P., Monge-Sanz, B.M., Morcrette, J.-J., Park, B.-K., Peubey, C., de Rosnay, P., Tavolato, C., Thépaut, J.-N., Vitart, F., 2011. The ERA-Interim reanalysis: configuration and performance of the data assimilation system. Q.J.R. Meteorol. Soc. 137, 553–597. https://doi.org/10.1002/qj.828.

DeMaria, M., Knaff, J.A., Connell, B.H., 2001. A tropical cyclone genesis parameter for the tropical Atlantic. Wea. Forecast. 16, 219–233. https://doi.org/10.1175/1520-0434(2001)016 < 0219:ATCGPF>2.0.CO;2.

Dvorak, V.F., 1975. Tropical cyclone intensity analysis and forecasting from satellite imagery. Mon. Weather Rev. 103, 420–430. https://doi.org/10.1175/1520-0493(1975)<0420:TCIAAF>2.0.CO;2.

Emanuel, K.A., 1986. An air-sea interaction theory for tropical cyclones. Part I: Steady-state maintenance. J. Atmos. Sci. 43, 585–605. https://doi.org/10.1111/1520-0469(1986)043<0585:AASITF>2.0.CO;2.

Evans, J.L., Guishard, M.P., 2009a. Atlantic subtropical storms. Part I: Diagnostic criteria and composite analysis. Mon. Weather Rev. 137, 2065–2080. https://doi.org/10.1175/2009MWR2468.1.

Evans, J.L., Guishard, M.P., 2009b. A proposed potential vorticity mechanism for subtropical cyclogenesis and tropical transition, p. 2.

Ferreira, R.N., Schubert, W.H., 1999. The role of tropical cyclones in the formation of tropical upper-tropospheric troughs. J. Atmos. Sci. 56, 17.

Font, I., 1983. Climatología de España y Portugal. Sección de publicaciones del Instituto Nacional de Meteorología, 296 pp. ISBN: 84–500–9467-4.

Galarneau, T.J., McTaggart-Cowan, R., Bosart, L.F., Davis, C.A., 2015. Development of North Atlantic tropical disturbances near upper-level potential vorticity streamers. J. Atmos. Sci. 72, 572–597. https://doi.org/10.1175/JAS-D-14-0106.1.

González-Alemán, J.J., Valero, F., Martín-León, F., Evans, J.L., 2015. Classification and synoptic analysis of subtropical cyclones within the North Atlantic Ocean*. J. Clim. 28, 3331–3352. https://doi.org/10.1175/JCLI-D-14-00276.1.

Gray, W.M., 1968. Global view of the origin of tropical disturbances and storms. Mon. Weather Rev. 96, 669–700. https://doi.org/10.1175/1520-0493(1968)096%3C0669:GVOTOO%3E2.0.CO;2.

Hersbach, H., Bell, B., Berrisford, P., Hirahara, S., Horányi, A., Muñoz-Sabater, J., Nicolas, J., Peubey, C., Radu, R., Schepers, D., Simmons, A., Soci, C., Abdalla, S., Abellan, X., Balsamo, G., Bechtold, P., Biavati, G., Bidlot, J., Bonavita, M., Chiara, G., Dahlgren, P., Dee, D., Diamantakis, M., Dragani, R., Flemming, J., Forbes, R., Fuentes, M., Geer, A., Haimberger, L., Healy, S., Hogan, R.J., Hólm, E., Janisková, M., Keeley, S., Laloyaux, P., Lopez, P., Lupu, C., Radnoti, G., Rosnay, P., Rozum, I., Vamborg, F., Villaume, S., Thépaut, J., 2020. The ERA5 global reanalysis. Q.J.R. Meteorol. Soc. 146, 1999–2049. https://doi.org/10.1002/qj.3803.

Hoskins, B.J., McIntyre, M.E., Robertson, A.W., 1985. On the use and significance of isentropic potential vorticity maps. Q.J.R. Meteorol. Soc. 111, 877–946. https://doi.org/10.1002/qj.49711147002.

Hoskins, B.J., Yang, G.-Y., Fonseca, R.M., 2020. The detailed dynamics of the June–August hadley cell. Q.J.R. Meteorol. Soc. 146, 557–575. https://doi.org/10.1002/qj.3702.

Hulme, A.L., Martin, J.E., 2009. Synoptic- and frontal-scale influences on tropical transition events in the Atlantic Basin. Part II: Tropical transition of hurricane karen. Mon. Weather Rev. 137, 3626–3650. https://doi.org/10.1175/2009MWR2803.1.

Knapp, K.R., Kruk, M.C., Levinson, D.H., Diamond, H.J., Neumann, C.J., 2010. The International Best Track Archive for Climate Stewardship (IBTrACS). Bull. Ame. Meteorol. Soc. 91, 363–376.

Landsea, C.W., Beven, J., 2019. The REVISED ATLANTIC HURRICANE DATABASE (HURDAT2). https://www.nhc.noaa.gov/data/hurdat/hurdat2-format-nov2019.pdf.

Landsea, C.W., Franklin, J.L., 2013. Atlantic hurricane database uncertainty and presentation of a new database format. Mon. Weather Rev. 141, 3576–3592.

Lenzen, M., Malik, A., Kenway, S., Daniels, P., Lam, K.L., Geschke, A., 2019. Economic damage and spillovers from a tropical cyclone. Nat. Hazards Earth Syst. Sci. 19, 137–151. https://doi.org/10.5194/nhess-19-137-2019.

Mann, H.B., Whitney, D.R., 1947. On a test of whether one of two random variables is stochastically larger than the other. Ann. Math. Stat. 18, 50–60.

Martius, O., Schwierz, C., Sprenger, M., 2008. Dynamical tropopause variability and potential vorticity streamers in the Northern Hemisphere – A climatological analysis. Adv. Atmos. Sci. 25, 367–380. https://doi.org/10.1007/s00376-008-0367-z.

Mauk, R.G., Hobgood, J.S., 2012. Tropical cyclone formation in environments with cool SST and high wind shear over the Northeastern Atlantic Ocean*. Weather Forecast. 27, 1433–1448. https://doi.org/10.1175/WAF-D-11-00048.1.

McIntyre, M.E., Palmer, T.N., 1983. Breaking planetary waves in the stratosphere. Nature 305, 593–600. https://doi.org/10.1038/305593a0.

McTaggart-Cowan, R., Deane, G.D., Bosart, L.F., Davis, C.A., Galarneau, T.J., 2008. Climatology of tropical cyclogenesis in the North Atlantic (1948–2004). Mon. Weather Rev. 136, 1284–1304. https://doi.org/10.1175/2007MWR2245.1.

McTaggart-Cowan, R., Galarneau, T.J., Bosart, L.F., Moore, R.W., Martius, O., 2013. A global climatology of baroclinically influenced tropical cyclogenesis. Mon. Weather Rev. 141, 1963–1989. https://doi.org/10.1175/MWR-D-12-00186.1.

McTaggart-Cowan, R., Davies, E.L., Fairman, J.G., Galarneau, T.J., Schultz, D.M., 2015. Revisiting the 26.5 °C sea surface temperature threshold for tropical cyclone development. Bull. Am. Meteorol. Soc. 96, 1929–1943. https://doi.org/10.1175/BAMS-D-13-00254.1.

Molinari, J., Vollaro, D., Bosart, L.F., Corbosiero, K.L., 2004. Tropical cyclone formation in a sheared environment: a case study. J. Atmos. Sci. 61–21, 2493–2509. https://doi.org/10.1175/JAS3291.1.

Muñoz, C., Schultz, D., Vaughan, G., 2020. A Midlatitude Circulation and Interannual Variability of 200- and 500-hPa Cut-Off Lows. J. Clim. 33, 2201–2222.

Nieto, R., Gimeno, L., de la Torre, L., Ribera, P., Gallego, D., García-Herrera, R., García, J. A., Nuñez, M., Redaño, A., Lorente, J., 2005. Climatological features of cutoff low systems in the Northern Hemisphere. J. Clim. 18, 3085–3103. https://doi.org/10.1175/JCLI3386.1.

Palmen, E., Newton, C.W., 1969. Atmospheric Circulation Systems: Their Structure and Physical Interpretation. Academic Press, p. 603.

Papin, P.P., Bosart, L.F., Torn, R.D., 2020. A feature-based approach to classifying summertime potential vorticity streamers linked to rossby wave breaking in the North Atlantic Basin. J. Clim. 33, 5953–5969. https://doi.org/10.1175/JCLI-D-19-0812.1.

Patla, J.E., Stevens, D., Barnes, G.M., 2009. A conceptual model for the influence of TUTT cells on tropical cyclone motion in the Northwest Pacific Ocean. Weather Forecast. 24, 1215–1235.

Peduzzi, P., Chatenoux, B., Dao, H., De Bono, A., Herold, C., Kossin, J., Mouton, F., Nordbeck, O., 2012. Global trends in tropical cyclone risk. Nat. Clim. Chang. 2, 289–294. https://doi.org/10.1038/nclimate1410.

Postel, G.A., Hitchman, M.H., 1999. A climatology of rossby wave breaking along the subtropical tropopause. J. Atmos. Sci. 56, 359–373. https://doi.org/10.1175/1520-0469(1999)056<0359:ACORWB>2.0.CO;2.

Raymond, D.J., 1992. Nonlinear balance and potential vorticity thinking at large Rossby number. Quart. J. Roy. Meteor. Soc. 118, 987–1015.

Sadler, J.C., 1976. A role of the tropical upper tropospheric trough in early season typhoon development. Monthly Weather Review 104, 1266–1278. https://doi.org/10.1775/1520-0493(1976)104<1266:AROTTU>2.0.CO;2.

Steward, S.R., 2018. Hurricane Ophelia (AL172017). National Hurricane Center - Tropical Cyclone Report.

Tapiador, F.J., Gaertner, M.A., Romera, R., Castro, M., 2007. A multisource analysis of hurricane vince. Bull. Am. Meteorol. Soc. 88, 1027–1032. https://doi.org/10.1175/BAMS-88-7-1027.

Taszarek, M., Allen, J.T., Púčik, T., Hoogewind, K.A., Brooks, H.E., 2020. Severe convective storms across Europe and the United States. Part II: ERA5 environments associated with lightning, Large Hail, Severe Wind, and Tornadoes. J. Clim. 33, 10263–10286. https://doi.org/10.1175/JCLI-D-20-0346.1.

Thorncroft, C.D., Hoskins, B.J., McIntyre, M.E., 1993. Two paradigms of baroclinic-wave life-cycle behavior. Q.J Royal Met. Soc. 119, 17–55. https://doi.org/10.1002/qj.49711950903.

Uppala, S.M., Kållberg, P.W., Simmons, A.J., Andrae, U., Bechtold, V.D.C., Fiorino, M., Gibson, J.K., Haseler, J., Hernandez, A., Kelly, G.A., Li, X., Onogi, K., Saarinen, S., Sokka, N., Allan, R.P., Andersson, E., Arpe, K., Balmaseda, M.A., Beljaars, A.C.M., Berg, L.V.D., Bidlot, J., Bormann, N., Caires, S., Chevallier, F., Dethof, A., Dragosavac, M., Fisher, M., Fuentes, M., Hagemann, S., Hólm, E., Hoskins, B.J., Isaksen, L., Janssen, P.A.E.M., Jenne, R., Mcnally, A.P., Mahfouf, J.-F., Morcrette, J.-J., Rayner, N.A., Saunders, R.W., Simon, P., Sterl, A., Trenberth, K.E., Untch, A., Vasiljevic, D., Viterbo, P., Woollen, J., 2005. The ERA-40 re-analysis. Q.J.R. Meteorol. Soc. 131, 2961–3012. https://doi.org/10.1256/qj.04.176.